Light Emitting Photon Upconversion Nanoparticles in the Generation of Transdermal Reactive Oxygen Species

Martin Prieto [a, ‡], Alina Y. Rwei [c, d, ‡], Teresa Alejo [a], Wei Tuo [c], Maria Teresa Lopez-Franco [a], Gracia Mendoza [a], Victor Sebastian [a, b], Daniel S. Kohane [c] Manuel Arruebo [a ,b,]**

[a] Department of Chemical Engineering. Aragon Institute of Nanoscience (INA), University of Zaragoza, Campus Río Ebro - Edificio I+D, C/ Poeta Mariano Esquillor S/N, 50018-Zaragoza, Spain; Aragon Health Research Institute (IIS Aragón), 50009 Zaragoza, Spain

[b] Networking Research Center on Bioengineering, Biomaterials and Nanomedicine, CIBER-BBN, 28029-Madrid, Spain.

[c] Laboratory for Biomaterials and Drug Delivery, Department of Anesthesiology, Boston Children's Hospital, Harvard Medical School, Boston, MA 02115.

[d] Department of Materials Science and Engineering, Massachusetts Institute of Technology, Cambridge, MA 02139.

‡: Both authors contributed equally to this work.

*: Corresponding authors: DSK (Daniel.Kohane@childrens.harvard.edu) and MA (arruebom@unizar.es)

ABSTRACT

Common photosensitizers used in photodynamic therapy do not penetrate the skin effectively. In addition, the visible blue and red lights used to excite such photosensitizers have shallow penetration depths through tissue. To overcome these limitations, we have synthesized ultraviolet and visible light emitting, energy-transfer based upconversion nanoparticles, and co-encapsulated them inside PLGA-PEG nanoparticles with photosensitizer protoporphyrin IX. Nd^{3+} has been introduced as sensitizer in the upconversion nanostructures to allow their excitation at 808 nm. The subcytotoxic doses of the hybrid nanoparticles have been evaluated on different cell lines (i.e., fibroblasts, HaCaT, THP-1 monocytic cell line, U251MG, and mMSCs cells). Upon NIR light excitation the upconversion nanoparticles emitted UV and VIS light which consequently activated the generation of reactive oxygen species (ROS). In addition, after irradiating at 808 nm, the resulting hybrid nanoparticles containing both upconversion nanoparticles and protoporphyrin IX generated 3.4 times more ROS than PLGA-PEG nanoparticles containing just the same dose of protoporphyrin IX. Their photodynamic effect was also assayed on different cell cultures demonstrating their efficacy to selectively kill treated and irradiated cells. Compared to the topical application of the free photosensitizer, an enhanced skin permeation penetration was observed for the nanoparticulate formulation using an ex vivo human skin permeation experiment. Whereas free protoporphyrin IX remained located at the outer layer of the skin, nanoparticle-encapsulated protoporphyrin IX was able to penetrate through the epidermal layer, slightly into the dermis.

KEYWORDS

Upconversion Nanoparticles, Photodynamic Therapy, PLGA-PEG, Protoporphyrin IX, Radical Oxygen Species.

INTRODUCTION

During the last decades, luminescent upconversion nanoparticles have been the focus of extensive research in the optoelectronics and biomedical fields due to their ability to convert near infrared (NIR) light to shorter wavelength light (VIS or UV), a process termed upconversion. The upconversion properties of these luminescence nanoparticles are attractive because in biomedical applications, NIR excitation is commonly used to maximize tissue penetration, minimize background autofluorescence and reduce photobleaching. However, UV or VIS light activates most of the photo-triggerable processes.

The UV and VIS light emitted by the upconversion nanoparticles together with the intrinsic characteristics of some activators (i.e., paramagnetic Gd^{3+}) have promoted the use of upconversion nanoparticles in various biomedical applications including fluorescence and magnetic resonance imaging, drug delivery, biosensing, and photodynamic therapy[1]. Photodynamic therapy using upconversion nanoparticles has been applied *in vitro* and *in vivo* in the treatment of tumors by using the VIS light generated by the nanoparticles in the activation of a photosensitizer located in close proximity to the upconversion nanoparticle which generates short-lived reactive oxygen species that eliminate cancer cells[2].

Drug and gene delivery systems have also been developed using the un-caging ability of the UV light generated by upconversion nanoparticles after NIR excitation. In this regard, Yan et al.[3] synthesized UV-responsive block copolymer micelles co-containing both upconversion

nanoparticles and dyes (i.e., Nile red). The NIR light excitation induced the generation of UV light by the caged upconverting nanoparticles, which consequently produced the photocleavage of specific labile groups of the micelle-forming block copolymer releasing the dye used as model payload. Photocaging of reporter and silencing genes has been demonstrated even *in vivo* using NIR-to-UV upconverting nanoparticles showing that it is feasible to obtain site-specific gene knockdown and patterning of biomolecules using externally applied NIR light[4,5]. Liu et al.[6] demonstrated the NIR-triggered anticancer drug release based on the use of upconverting nanoparticles coated with a mesoporous silica shell containing the drug and using the trans–cis photoisomerization of azobenzene molecules as molecular gates. In this case, upon NIR light illumination the UV light generated by the upconverting crystal triggered the photoisomerization and consequent drug release. Multifunctional platforms have also been reported combining the ability of the NIR-to-UV upconversion nanoparticles to simultaneously trigger drug release and also monitor the presence of the nanoparticles in the tissues[7,8]. In addition, multimodal bioimaging using computed tomography, upconversion luminescence and magnetic resonance imaging together with photodynamic effects have been demonstrated using mesoporous silica coated upconversion nanoparticles containing two different photosensitizers[9].

The localization of the drug on the affected area, its reduced side effects, and non-invasive character make topical drug administration advantageous over other administration routes. In photodynamic therapy, the topical delivery of organic photosensitizers is limited by their intrinsic photobleaching together with their low permeance through the epidermis. To facilitate the permeation through the intracellular lipids (i.e., neutral lipids and sphingolipids) of the stratum corneum, the photosensitizer carrier should have a pH similar to that of the skin (i.e., 5.5) and intrinsic hydrophobicity to avoid agglomeration. Nanoparticulate systems encapsulating both

hydrophilic and hydrophobic photosensitizers can overcome those limitations to favor the accumulation of the dye into the dermis. In photodynamic therapy blue and red light are commonly used to generate reactive oxygen species (ROS); however these VIS wavelengths show shallow penetration depths[10] whereas NIR light shows higher penetration into the tissues[11]. In order to overcome the limited topical penetration of photosensitizers and the reduced penetration depth of the VIS light commonly used in photodynamic therapy, herein, energy transfer-based upconversion nanoparticles based on Yb^{3+} as sensitizer and varied activators (i.e., Tm^{3+}, Er^{3+}, Gd^{3+}, etc.) emitting VIS and UV light after being excited with NIR light have been prepared. Those nanoparticles have been co-encapsulated inside PLGA-PEG nanoparticles containing also the endogenous photosensitizer protoporphyrin IX, commonly used in actinic keratosis and skin cancers. ROS generation after NIR light irradiation at 808 nm using an *ex vivo* skin permeation experiment has been successfully demonstrated. Hence, the current limitations of photodynamic therapy that include the reduced penetration of hydrophilic photosensitizers (e.g., 5-aminolevulinic acid), their quick photobleaching, and also the shallow penetration depth of the visible light commonly applied during treatment can be overcome by encapsulating hydrophobic forms of the photosensitizer (i.e., protoporphyrin IX) combined with upconversion nanoparticles which allow using highly penetrant NIR light to trigger the generation of reactive oxygen species. Therefore, we demonstrate that using upconversion nanoparticles it is possible to employ externally applied NIR light to generate UV or VIS light underneath the skin and trigger the activation of a photosensitizer in close proximity to the upconverting nanoparticles with the consequent ROS generation. In addition, enhanced photosensitizer skin permeation was reached thanks to its nanoencapsulation in a polymeric matrix.

RESULTS AND DISCUSSION

Synthesis of PLGA-PEG nanoparticles co-containing upconversion nanoparticles and protoporphyrin IX. Figure 1 shows the morphology of the upconverting crystals resulting from the solvothermal synthesis. TEM photographs show the $NaYF_4$:Yb^{3+} crystals with a characteristic thermodynamically stable hexagonal structure (β phase), which was corroborated by high-resolution scanning transmission electron microscopy (STEM) and by XRD analysis (Figure S1a). By tilting the TEM holder we observed a hexagonal flat plate structure characteristic of a NaF/Yb^{3+} molar ratio of 8 in agreement with the previous literature[12]. Particle sizes of 41.1±2.3 nm were measured from the TEM images (N=250). Core and shell are not distinguishable by TEM because of their close crystalline structures and compositions as previously reported[13], but shell size could be determined by subtracting the total size from the core mean diameter (Figure 1a), showing a mean thickness of 22.3±2.6 nm. Oleic acid, chemisorbed onto the surface of the upconversion nanoparticles via its carboxylate group, acts as solvent and stabilizer preventing the resulting nanoparticles from agglomeration in organic solvents[14]. During TEM observation, long-range ordered structures were observed after drying the particles, corroborating the presence of the oleic acid on the nanoparticle surfaces. EDX analysis (Figure S1b) confirmed the presence of the elements of the host matrix (i.e., $NaYF_4$), the sensitizer (Yb^{3+}), the activator and accumulator (Tm^{3+}) and also Nd^{3+} (to promote energy transfer to the activator, i.e., Yb^{3+}, and the consequent absorption at 808nm as we mentioned before).

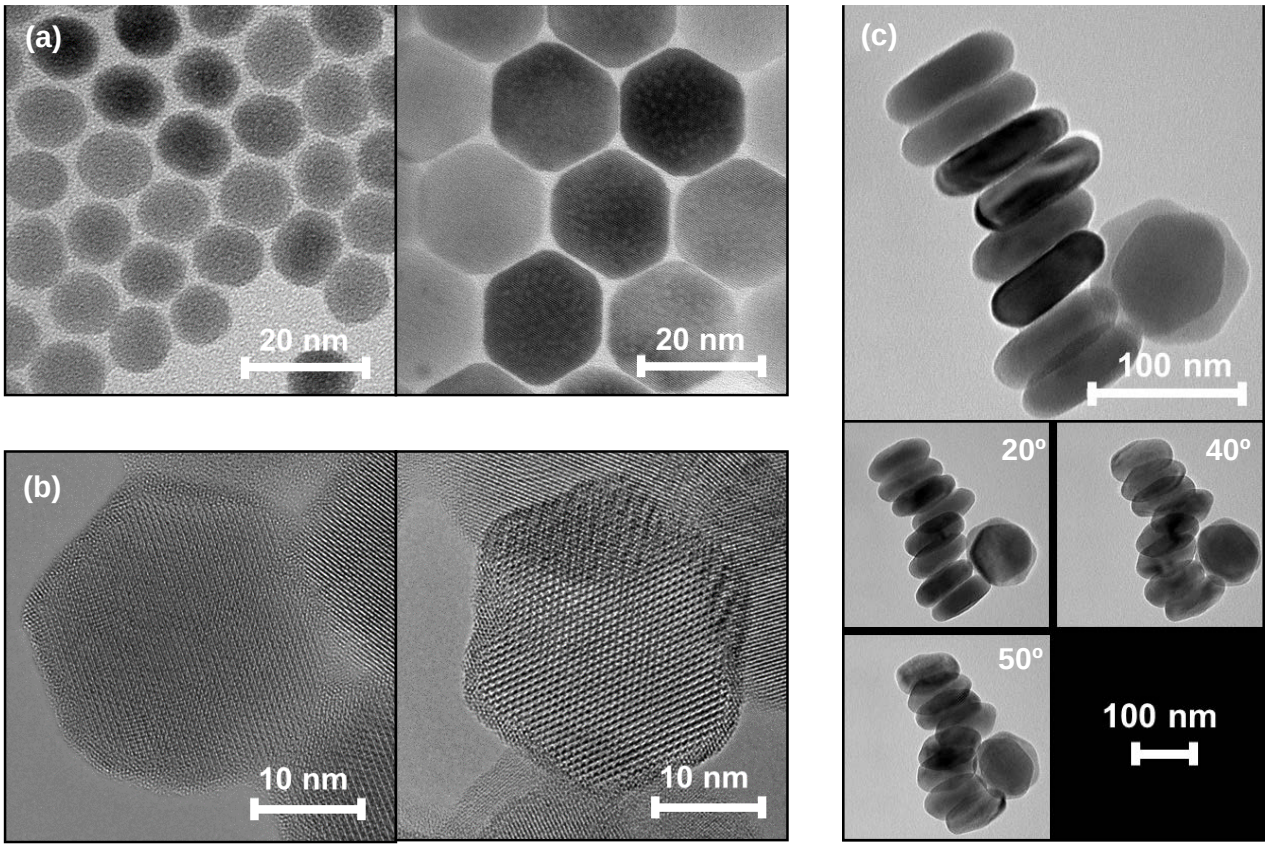

Figure 1. (a) TEM images of the core (left) composed of β-$NaYF_4$: Gd, Yb, Nd, Tm and the final core-shell nanoparticles (right) composed of β-$NaYF_4$: Gd, Yb, Nd, Tm/$NaYF_4$:Nd and (b) HRTEM images of a single core-shell nanocrystal; (c) Side view of one core-shell nanocrystal from different tilt angles revealing the hexagonal nanoplate structure.

Gd^{3+} was also incorporated and detected in the nanoparticle core to achieve UV emission and to enhance upconversion luminescence thanks to its fast energy migration and because its excited and ground states are separated by a relatively large energy gap which reduces energy losses by multiphonon emission and cross-relaxation[13]. In addition, excited Gd^{3+} states showed high order upconversion emissions in the UV region (i.e., 311.7 nm) due to the $^6P_{7/2}$-$^8S_{7/2}$ transitions[15]. The emissions generated by the nanoparticles after excitation at 980 and 808 nm are depicted in Figure 2, as well as their corresponding energy transfers (Figure S1c). These nanoparticles showed a 3-

and 4-order of the upconversion process after calculating the slope of the luminescence intensity versus different pump powers in double-logarithmic representation[16] (Figure S2). This means that for those core-shell nanoparticles the emissions in the VIS and UV regions of the electromagnetic spectrum are 3- and 4-photon processes, respectively[17,18]. This indicates that to up to 4 photons are absorbed simultaneously by the sensitizer and one of its electrons promoted from a lower energy level to a higher one. In this case, Yb^{3+} acts as sensitizer because it shows of all lanthanide ions the largest absorption cross section at 980 nm (near infrared wavelength usually employed to excite those materials) due to $^2F_{7/2}$-$^2F_{5/2}$ transitions, acting other lanthanides as activators of the upconversion emission thanks to the resonant character of their f-f transitions with the Yb^{3+} transitions[19]. Nd^{3+} was also introduced as sensitizer in the resulting core-shell upconversion nanostructures to allow their excitation at 808 nm (common wavelength used in photothermal therapy) and simultaneous energy transfer to Yb^{3+} thanks to the multiple excitation bands that Nd^{3+} shows at 730, 808, and 865 nm, corresponding to transitions from $^4I_{9/2}$ to $^4F_{7/2}$, $^4F_{5/2}$, and $^4F_{3/2}$, respectively[20].

Figure 2a shows the optical emission of the upconverting crystals in ethanol where the predominant blue emission (at 450-480nm) is clearly observable when irradiated with 980 and 808 nm wavelength lasers. In addition, this emission was preserved in water after nanoparticle surface functionalization with polyethylenglycol thiol (SH-PEG). The absorption spectrum of the nanoparticles (Figure 2b) showed absorbance at 808 and 980 nm and large scattering at short wavelengths but reduced scattering in the NIR region, which represents the possibility of achieving deep tissue penetration.

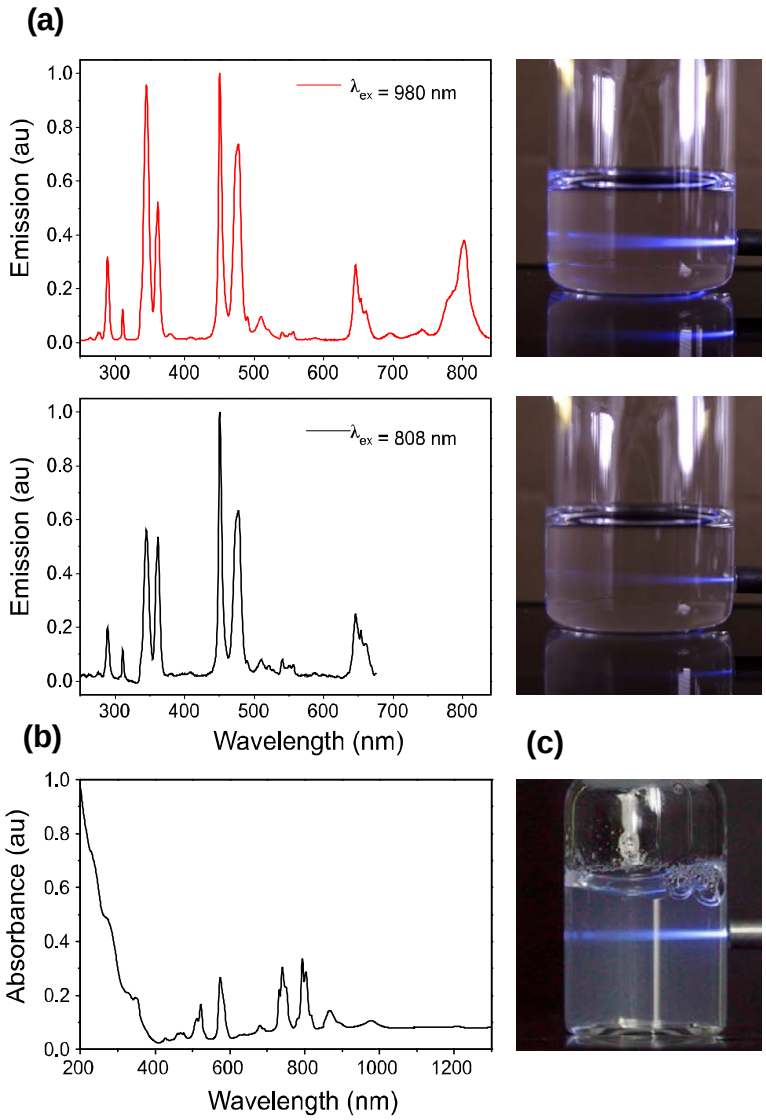

Figure 2. (a) Normalized emission spectra under excitation at 980 nm (top) and 808 nm (bottom) and their respective luminescence photographs of vials with the nanoparticle dispersions. The spectra and photographs were recorded in ethanol (1 mg/mL) using a power of 350 W/cm^2. (b) UV-Vis absorbance spectrum of the resulting core-shell nanoparticles composed of β-$NaYF_4$: Gd, Yb, Nd,

Tm/$NaYF_4$:Nd. (c) luminescence photograph of PEG functionalized core-shell nanoparticles (1 mg/mL) dispersed in water and contained in a vial.

As described in the Materials and Methods section, PLGA-PEG nanoparticles containing upconversion nanoparticles were prepared by nanoprecipitation using miscible solvents (water and tetrahydrofuran, THF). Aqueous dispersions (10 mg/mL) of PLGA-PEG nanoparticles containing upconversion nanoparticles (28.6 ± 0.8 wt.%, measured by thermogravimetric analysis, TGA) did not produce blue emission visible to the naked eye after NIR (808nm) irradiation (530 W/cm^2); however their resulting freeze-dried powders did (Figure S3). Hence, the upconversion emission remained inside the PLGA-PEG nanoparticles after encapsulating the upconversion nanoparticles. In addition to the light scattering caused by the PLGA-PEG nanoparticles, water quenches upconversion emission due to the energy transfer between the upconverting crystal and the water molecules and because of the excitation energy depletion that water produces due to its inherent absorption (although reduced) in the NIR region[21]. Those reasons might explain why the emission was not observable to the naked eye when using the colloidal water-based suspension but it was clearly observed when using its resulting freeze-dried powders. With the same upconversion-nanoparticle loading (28.6 ± 0.8 wt.%) inside PLGA-PEG, lyophilized powders of PLGA-PEG nanoparticles containing both protoporphyrin IX and upconversion nanoparticles did not show any emission under the same irradiation conditions which could be attributed to the light absorption caused by the protoporphyrin IX (Figure S2). This is not surprising considering that light emission is generated in close proximity to the production site. Hence, after irradiating at 808 nm (530 W/cm^2) the upconversion emission of the inner lanthanide-based crystals was absorbed by the closely packed porphyrin. This dye shows a maximum absorption in the blue (440-480nm)

and red (650-800nm) regions of the electromagnetic spectrum[22], which overlaps with the emission of the upconversion crystals (maximum at 477, 451 and 647-661nm, Figure S1c).

PLGA-PEG nanoparticles containing both protoporphyrin IX and upconversion nanoparticles are depicted in Figure 3. The particle size of the final hybrid nanoparticles was 288.1 ± 49.2 nm measured by TEM (N=50). Encapsulation efficiencies of 6.24 ± 0.8 wt. % (ratio between the measured protoporphyrin IX mass and the mass of protoporphyrin added in the synthesis) and drug loadings of 0.22 ± 0.03 wt. % (ratio between the measured protoporphyrin IX mass and the mass of PLGA-PEG, calculated by TGA) were calculated by fluorescence spectroscopy (λ_{ex}=400nm, λ_{em}=630nm) following a previously reported protocol[23].

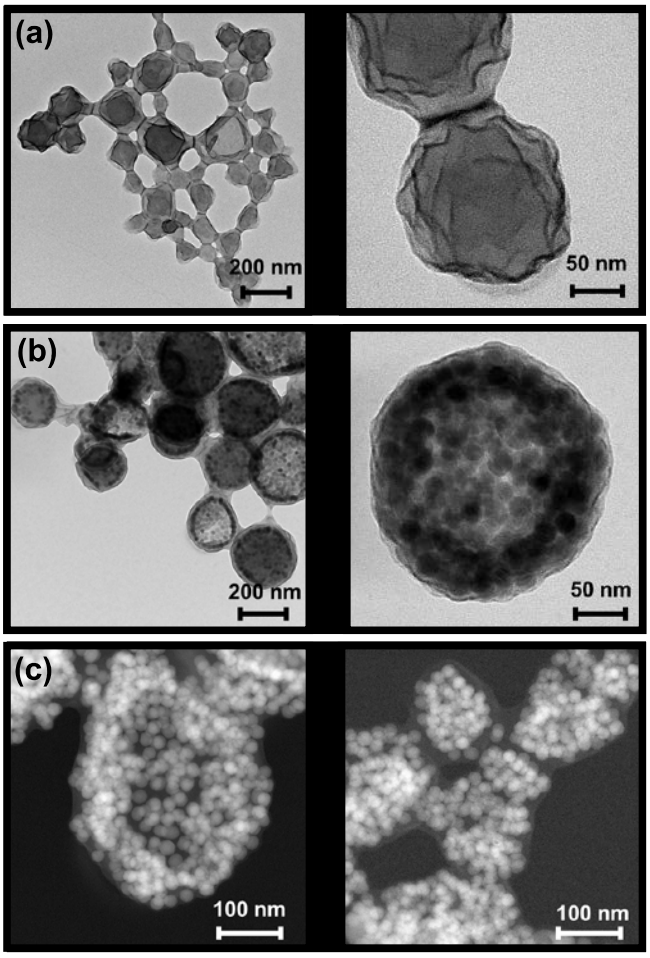

Figure 3. (a) TEM images of PLGA-PEG nanoparticles obtained by nanoprecipitation. (b) TEM and (c) STEM-HAADF images of PLGA-PEG NPs containing both core-shell UCNPs (28.6 ± 0.8 wt.%) and protoporphyrin IX (0.22 ± 0.03 wt.%).

The inner upconversion crystals were clearly visualized under TEM due to their high electron density. The size of the final hybrid nanoparticles is still lower than the maximum sizes (< 200-300 nm) reported for the topical delivery of protoporphyrin IX (or 5-aminolevulinic acid, which is the protoporphyrin IX endogenous precursor in the porphyrin synthesis pathway). Reduced

nanoparticle sizes would favor the topical delivery of the porphyrin through the lipid stacks located between the proteinaceous dead cells (i.e., corneocytes) of the stratum corneum.

Free radical generation by the hybrid nanoparticles. ROS generation after 980nm-light irradiation was evaluated by collecting the emission of R123 (rhodamine 123) at 530 nm in the presence of the non-encapsulated upconversion nanoparticles. The heating rate upon the laser irradiation on upconversion nanoparticles under the presence of DHR123 (Dihydrorhodamine 123) was evaluated in order to decouple the photothermal effect from the photochemical effect that was exerted on the dye. Figure 4a shows that the colloidal nanoparticle suspension (5 mg/mL) reached 50ºC (ΔT=26ºC) in 8 min upon laser irradiation (11 W/cm^2; such high irradiance was used to obtain a fast response). Under the same irradiation conditions an ethanolic solution of DHR123 without the nanoparticles showed a temperature increase of ΔT=13ºC. Heating at 50ºC by applying the laser or having the presence of upconverting nanocrystals (5 mg/mL) did not induce DHR123 degradation, showing the same fluorescence intensity irrespectively of the exposure time (Figure S4) in agreement with the previous literature[24]; however, the presence of nanoparticles and heating simultaneously promoted DHR123 oxidation (Figure 4b). This phenomenon could be partially explained by the generation of reactive nitrogen species after heating water under the presence of DHR123, as previously reported[25]. This reaction could be potentially catalyzed by the presence of the lanthanide nanocrystals. Upconversion nanoparticles irradiation at 980 nm induced free radical generation 1.2 times greater than the heating of the nanoparticles alone did. This is indicative of the ROS generation by the upconverting crystals probably caused by the UV and VIS light they produce as previously reported[2]. The irradiation of the DHR123 dissolved in ethanol without nanoparticles did not induce ROS generation (Figure S4, top right). Hence, the upconversion nanoparticles themselves were able to produce ROS after

NIR light irradiation and these free radicals could potentially be used to cause photo-oxidation of malignant cells.

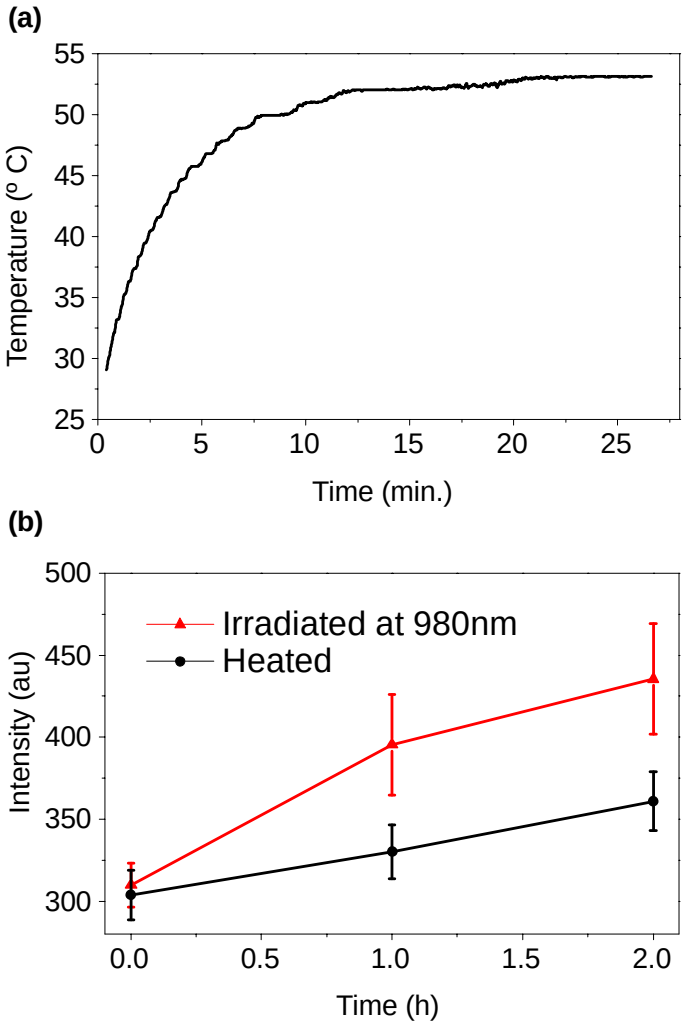

Figure 4. (a) Heating rate under laser irradiation (980 nm, 11 W/cm2) of a colloidal suspension in ethanol (1 mL) of the upconversion nanoparticles (5 mg/mL) and (b) DHR123 fluorescence emission at 530 nm after irradiation and heating at different times in a colloidal suspension (5 mg/mL) of UCNPs (three independent replicas).

Determination of the sub-cytotoxic dose of the hybrid nanoparticles and *in vitro* photodynamic effects. *In vitro* cytotoxicity of the synthesized nanoparticles was measured against different cell lines (Figure 5). Oleic-acid capped (Figure 5a) and SH-PEG functionalized (Figure 5c) upconversion nanoparticles did not display cytotoxic effects up to 0.4 mg/mL on the five cell lines assayed showing viabilities above 70%. The interference of the nanoparticles at the highest concentration with the assay was evaluated and discarded. Even much higher doses of similar upconversion nanoparticles have shown no toxic effect on different animal models[26]. PLGA-PEG nanoparticles containing upconversion nanoparticles only or containing both protoporphyrin IX and upconversion nanoparticles were also found to be noncytotoxic[27] at the concentrations tested (0.01-0.4 mg/mL) on fibroblasts and keratinocytes. A similar finding was demonstrated with the unloaded PLGA-PEG NPs. On the other hand, macrophage viability slightly decreased ($p < 0.005$) below 70% cell viability after treatment with PLGA-PEG nanoparticles containing upconversion nanoparticles. The macrophage viability also decreased after treatment with PLGA-PEG nanoparticles containing both upconversion nanoparticles and protoporphyrin IX compared to the control (untreated) samples (Figure 5d), which may be attributed to the phagocytic role of this cell line[28] so their NP uptake may be higher compared to the other cells assayed. However, the morphology of macrophages remained unaltered after being in contact with the oleic-acid capped nanoparticles (0.01 and 0.4 mg/mL) for 24 h, which could be another indication of the cytocompatibility of the upconversion nanoparticles at the doses tested (Figure 5b). We chose macrophages for SEM observation because of the elevated nanoparticle phagocytic uptake of this cell line. The cell survival exerted by the upconversion nanoparticles above 60-70% was attributed to their low water solubility and consequent reduced cellular contact of the oleic acid-caped nanoparticles in one case and to the buffering effect that PEG produces on

the cytotoxicity of the nanoparticles avoiding direct cell contact and internalization on the other case.

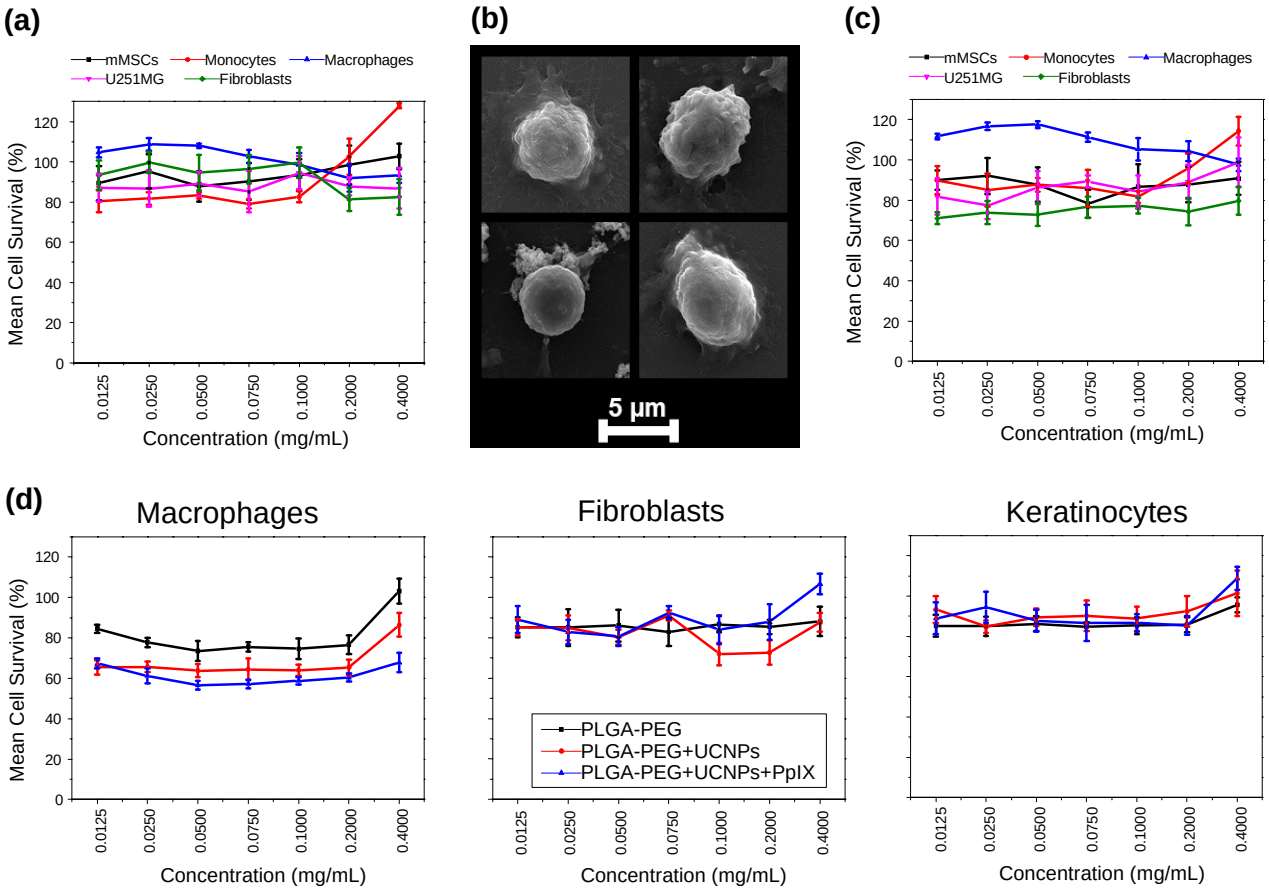

Figure 5. Viability assay using five cellular lines of (a) oleic-acid capped and (c) SH-PEG functionalized upconversion nanoparticles. (b) SEM images of macrophages incubated for 24h with oleic-acid capped upconversion nanoparticles at 0.01 mg/mL (top-right) and 0.04 mg/mL (bottom-left), SH-PEG functionalized upconversion nanoparticles at 0.01 mg/mL (bottom-right) and control (top-left) (d) Viability comparison between PLGA-PEG NPs, upconversion nanoparticles encapsulated in PLGA-PEG and PLGA-PEG NPs containing upconversion nanoparticles and Protoporphyrin IX, using three different cell lines. Control samples (not treated cells) were set as reference of viability (100%). N=5.

Several studies have shown the low toxicity of upconversion nanoparticles mainly against tumoral cells and macrophages[26], though, to the best of our knowledge, their toxicity against fibroblasts and keratinocytes has not been shown before. The treatment of human gastric cancer cells with lanthanide nanoparticles for the photodynamic treatment of tumors did not display high cytotoxicity except for the highest concentration assayed (1 mg/mL) of a mixture composed of protoporphyrin IX and lanthanide nanoparticles. However, this cytotoxicity was only observed after NIR irradiation, and it was attributed to the singlet oxygen generation and the subsequent photodynamic cellular damage[29]. In this regard, the addition of upconversion nanoparticles functionalized with α-cyclodextrin to A-549 cells resulted in high viability at values up to 0.4 mg/mL, showing again their high ability to produce cytotoxic singlet oxygen after NIR irradiation[30]. The cytotoxic effects of PEGylated upconversion nanoparticles were assessed against human liver cells and murine macrophages as nanoparticles are prone to be accumulated in the liver and spleen after IV administration, exerting high viability percentages (>82%) at concentrations between 0.05 and 1.6 mg/mL[31].

Photodynamic effects derived from ROS generation on different cell types, such as melanoma cells (B16F1), mouse mesenchymal stem cells (mMSCs), human dermal fibroblasts and human macrophages, were also tested (Fig. 6, Fig. S5 and Fig S6) by fluorescence microscopy after staining live cells with calcein and dead cells with ethidium bromide. After 20 minutes irradiation on melanoma cells treated with PLGA-PEG NPs containing upconversion NPs and protoporphyrin, oxidative damage was immediately detected in the irradiated area (Fig 6a) showing a central area of dead cells (red) corresponding with the laser spot surrounded by live cells (green). The temperature of the culture was monitored and no temperature increase was observed, discarding any thermal mediated cell damage. Samples irradiated at shorter times (5 and

10 min) needed 24h to clearly exert oxidative cell damage (Fig 6b and 6c), underlining the dependency on the irradiation time to obtain an accentuated cellular damage by biomolecule photooxidation[32]. It should be noted that after 24h, samples irradiated for 20 minutes did not contain cells, suggesting an extensive cell death and detachment. Furthermore, control samples, both treated and/or irradiated with the separated components of the final NPs (PLGA-PEG NPs, upconversion NPs and protoporphyrin IX), did not exert oxidative damage (Fig S5), and the increase in the temperature of the cell wells was always < 2 ºC (data not shown), pointing to the restricted photodynamic effect of the final nanomaterials mediated by ROS. The other cell types assayed also displayed cell death mediated by ROS after 24h when treated with PLGA-PEG NPs containing upconversion nanoparticles and Protoporphyrin IX after irradiation, being more accentuated in the phagocytic cell type (macrophages) than in mesenchymal and fibroblast cells (Fig S6). Different nanoparticles are commonly used to generate photodynamic effects[33,34]; but these results highlight the photodynamic effect of our NPs showing high viability when cells were not irradiated though displaying an extensive oxidative cell damage and subsequent death after NIR irradiation. In this line, previous works have shown the effects of photodynamic therapy mediated by NIR irradiation on tumor cells treated with the photosensitizer protoporphyrin mediated by its precursor 5-aminolevulinic acid (ALA). A431 squamous carcinoma cell monolayers and 3D cultures were treated with ALA in order to obtain PPIX, and subsequently irradiated (LED light at 15 mW)[35]. The evaluation of the samples 24h after irradiation showed a central spot of dead cells consistent with our studies. Cell viability of different tumor cells (i.e., AtT-20 and U373) treated with ALA also showed a decrease 12-14h after irradiation though this treatment on GH3 cells, which present an additional mechanism for protoporphyrin efflux, did not exert changes in cell viability[36]. Also, the efficient photodynamic effects of ALA treatment to

obtain PPIX on dormant PC-3 prostate cancer spheroids, which accumulate high levels of PPIX, were clearly demonstrated through the high cell mortality displayed 24h after irradiation[37].

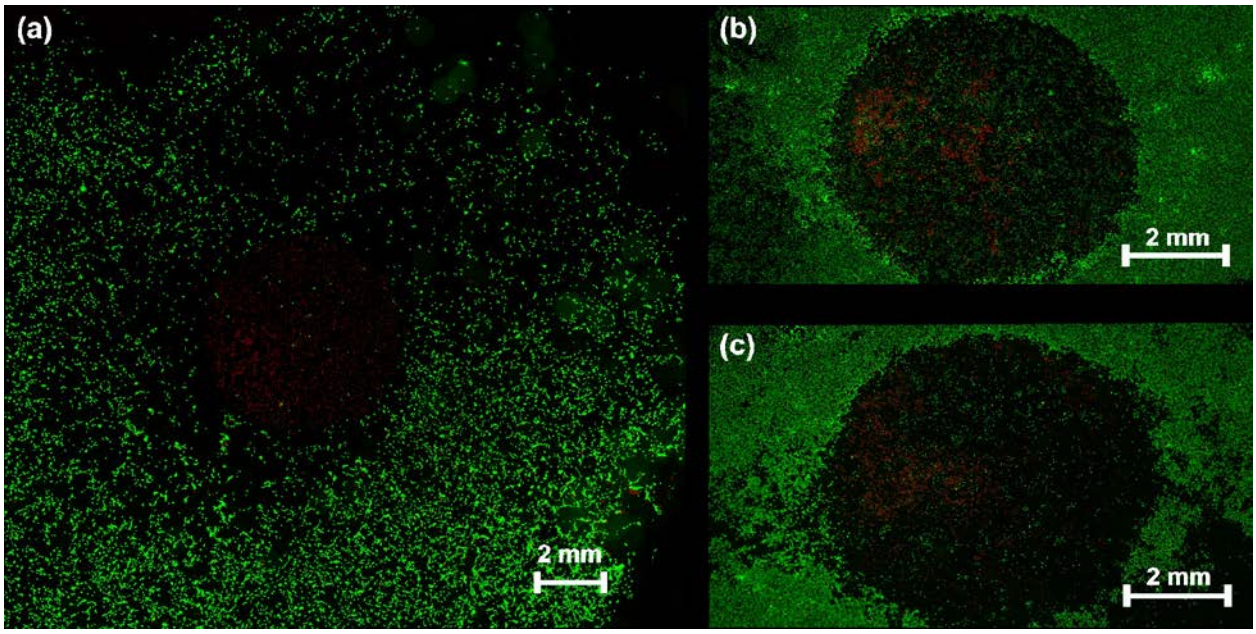

Figure 6. Photodynamic effects on murine melanoma cells (B16F1 cell line). Composition of pictures (4X magnification) obtained by fluorescence microscopy to show the whole culture well when cells were treated for 24h with PLGA-PEG NPs containing upconversion nanoparticles and Protoporphyrin IX. (a) B16F1 cells laser irradiated (808 nm) for 20 min and images acquired immediately after irradiation; (b and c) B16F1 cells laser irradiated for 5 min (b) and 10 min (c) and images acquired 24h after irradiation. Live cells are stained in green while dead cells in red.

Thus, the biomedical potential of upconversion nanoparticles lies in producing no cytotoxicity without light activation, but this can be triggered by means of NIR irradiation and consequent singlet oxygen production displaying their photodynamic therapeutic effects.

***Ex vivo* skin permeation experiment.** Singlet oxygen generation using the singlet oxygen sensor green revealed that after irradiating at 808nm (800 mW/cm^2) the PLGA-PEG nanoparticles

containing both upconversion nanoparticles and protoporphyrin IX generated 3.4 times more singlet oxygen than PLGA-PEG nanoparticles containing just the same dose of protoporphyrin IX (Figure S7). These results suggest that the co-encapsulation of UCNP effectively excited protoporphyrin IX and enhanced the generation of singlet oxygen from protoporphyrin IX-loaded particles. PLGA-PEG nanoparticles containing upconversion nanoparticles without protoporphyrin IX did not generate ROS at concentrations above the detection limit of the fluorometer, showing that the observed enhancement of singlet oxygen generation in Figure S7 was not due to the ROS generation from the UCNP itself. Again, due to the short half-life of ROS, they are only effective when located very close to the production site[38] and accordingly we demonstrated that the activation of the upconversion nanoparticles generates enough emitted light to trigger the oxidative free radicals from the closely located protoporphyrin IX.

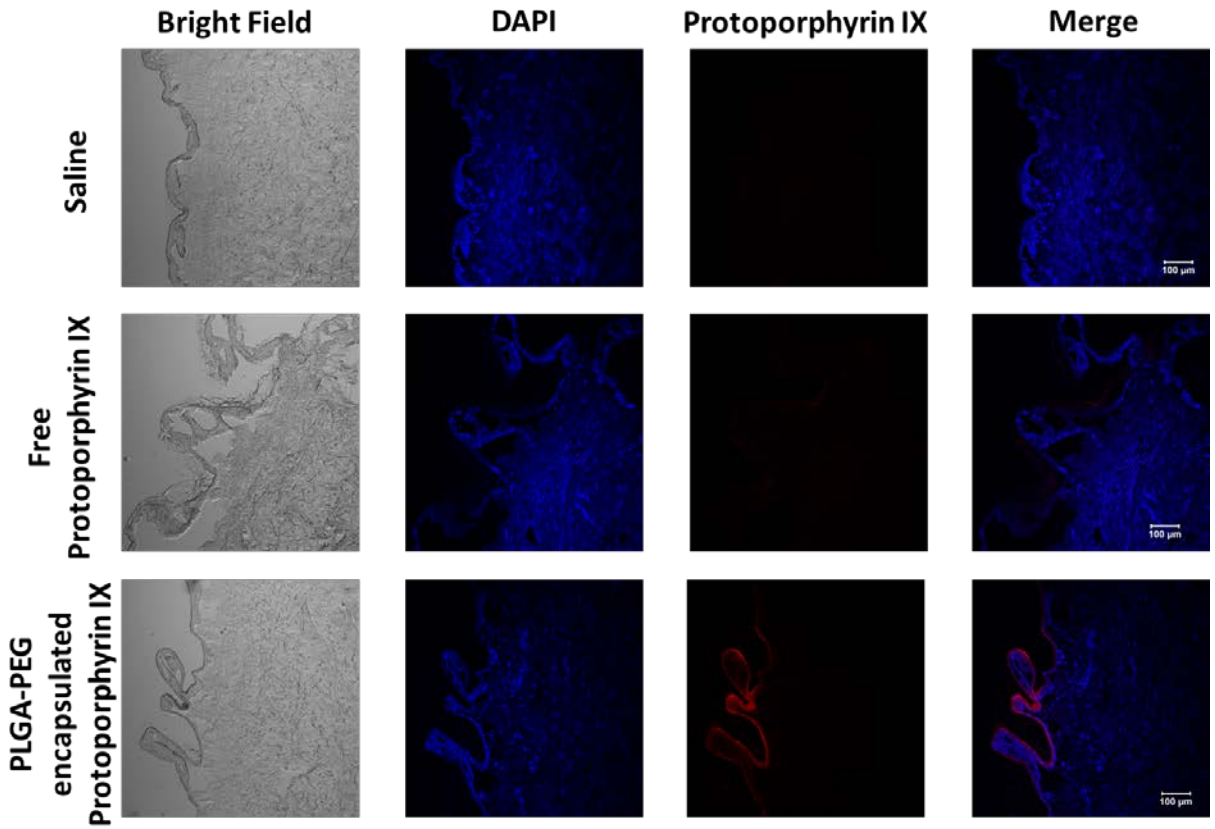

Figure 7. Confocal laser scanning microscopy images of the skin penetration test.

The PPIX-loaded nanoparticles were placed onto human skin and the skin penetration properties of these nanoparticles were studied using a Franz Diffusion Cell. The skin permeation test revealed that whereas free protoporphyrin IX was unable to permeate through the skin after 24 h at room temperature, once encapsulated within the PLGA-PEG polymeric nanoparticles the dye was able to permeate the epidermis layer and reach into the dermis (Figure 7). The reduced skin permeability of free protoporphyrin IX could be attributed to its aggregation at the pH of the skin[39], which can be improved by using penetration enhancers, by chemical modification or by encapsulation as here reported. These results demonstrate that the nanoparticulate form of protoporphyrin IX may be a promising approach for the topical delivery of photosensitizers.

CONCLUSIONS

Core-shell upconversion nanoparticles are able to induce ROS generation upon 808nm-NIR light irradiation. Co-encapsulation of upconversion nanoparticles and photosensitizers inside PLGA-PEG nanoparticles allows transdermal delivery and an enhanced ROS generation (3.4 times greater) compared to that achieved with just the encapsulated photosensitizer. The photodynamic effect of those nanoparticles was also demonstrated *in vitro* producing ROS mediated damage in cells. By confocal laser scanning microscopy we have demonstrated that free lipophilic protoporphyrin IX remains mainly on the top skin layer but the PLGA-PEG encapsulated one penetrates through the epidermal layer, slightly into the dermis.

MATERIALS AND METHODS

PLGA-PEG Resomer® RGP d5055 was purchased from Evonik Industries AG (Germany). Protoporphyrin IX (95%), Yttrium (III) chloride hexahydrate (99.99%), Neodymium (III) chloride (99.9%), Thulium (III) chloride (99.9%, Gadolinium (III) chloride hexahydrate (99.99%), Ytterbium (III) chloride hexahydrate (99.998%), Oleic acid (90%), 1-octadecene (90%), Ammonium Fluoride (98%), sodium hydroxide (98%) and dihydrorhodamine 123 (95%) were all purchased from Sigma-Aldrich and used as received. All other chemicals were also purchased from Sigma-Aldrich unless otherwise noted.

Synthesis of β-$NaYF_4$: Gd, Yb, Nd, Tm cores. 8 mL of a 0.2M aqueous solution of YCl_3, $GdCl_3$, $YbCl_3$, $NdCl_3$ and $TmCl_3$ (lanthanide ion molar ratio: Y/Gd/Yb/Nd/Tm = 58.5:20:20:1:0.5) was mixed with 24 mL of 1-octadecene and 16 mL of oleic acid in a 250 mL three-neck round bottom flask. The mixture was heated slowly (3 ºC/min) under stirring to 170 ºC to remove water and to produce oleate complexes, and then cooled down to room temperature. 4 mL of a sodium hydroxide solution in methanol (1M) was mixed with 13.2 mL of an ammonium fluoride solution in methanol (0.4M) and immediately added to the cooled reaction. The flask was stirred at room temperature for 40 minutes and then heated to 100 ºC (15 ºC/min) under vacuum to completely remove the methanol. Finally, the reaction was heated to 305 ºC (15 ºC/min), maintained at this temperature for 90 minutes and cooled to room temperature. The synthesis was protected from oxidation by a constant flow of dry argon throughout the process. Core nanoparticles were then collected from the reaction flask by centrifugation (6000 rpm/10 min) after adding 60 mL of ethanol and finally dispersed in 16 mL of cyclohexane.

Synthesis of β-$NaYF_4$: Gd, Yb, Nd, Tm / $NaYF_4$: Nd core-shell structures. 8 mL of a 0.2M aqueous solution of YCl_3, $NdCl_3$ (lanthanide ion molar ratio: Y/Nd = 8:2) was mixed with 24 mL

of 1-octadecene and 16 mL of oleic acid in a 250 mL three-neck round bottom flask. The mixture was heated slowly under stirring to 170 ºC (3 ºC/min) to remove water and to produce oleate complexes, and then cooled down to room temperature.

The previously synthesized core nanoparticles were transferred to the reaction flask and stirred for 5 minutes. Then, 4 mL of a sodium hydroxide solution in methanol (1M) was mixed with 13.2 mL of an ammonium fluoride solution in methanol (0.4M) and added immediately. The flask was stirred at room temperature for 40 minutes and then heated to 100 ºC (15 ºC/min) under vacuum to completely remove the methanol and cyclohexane. Finally, the reaction was heated to 305 ºC (15 ºC/min) maintained at this temperature for 90 minutes and cooled down to room temperature. The synthesis was also protected from oxidation by a constant flow of dry argon throughout the process. The final product was collected from the reaction by centrifugation (6000 rpm/10 min) after addition of 60 mL of ethanol, purified by two cycles of centrifugal washing in cyclohexane (12000 rpm/20 min) and dried under vacuum.

The resulting nanoparticles were ligand-exchanged with polyethylene glycol thiol to render them water-soluble. Different strategies have been followed to carry out this direct exchange including click chemistry[40], In our case, we removed the oleic acid coating according to the following protocol: the oleic-acid capped nanoparticles were first re-dispersed in HCl aqueous solution (0.1 M) at a concentration of 10 mg/mL and sonicated for 20 minutes to detach the oleic acid by repeating this procedure 3 times. The uncapped nanoparticles were dried under vacuum and dispersed in water at a final concentration of 2 mg/mL and reacted with polyethylene glycol methyl ether thiol (SH-PEG, 800 Da, 2mg/mL) in a volume ratio of 1:1, and stirred for one hour. Finally, PEGylated upconversion nanoparticles were washed by several centrifugation cycles in water (10000 rpm/20 min) to remove unbound SH-PEG. Thiol forms a dative bond with metal

atoms due to the lone pair of electrons on the sulfur atom and the PEG corona provides the nanoparticles with steric hindrance and increases the hydrophilicity via ether repeat units, which form hydrogen bonds with water[41].

Upconversion nanoparticles and protoporphyrin IX encapsulation in PLGA-PEG. Upconversion nanoparticles and protoporphyrin IX were co-encapsulated in PLGA-PEG using a nanoprecipitation method. Briefly, 5 mg of PLGA-PEG, 5 mg of core-shell upconversion nanoparticles and 250 µg of protoporphyrin IX were dissolved in 1 mL of tetrahydrofuran (THF). This dispersion was added drop-wise at 2 mL/h using a syringe pump (model PHD Ultra, Harvard Apparatus, Holliston, MA, USA) over 1 mL of milli-Q water magnetically stirred (380 rpm). Then, THF was evaporated by magnetic stirring at room temperature for 2 hours and nanoparticles were purified to remove leftover THF and non-encapsulated protoporphyrin IX by four cycles of centrifugal washing in milli-Q water (6000 rpm/10 min).

Nanoparticle characterization. Optical characterization measurements were performed using an optical setup consisting of a quartz cell (High precision Suprasil® quartz cell, Hellma GmbH and Co. KG, Mullheim, Germany) with two coplanar optical fibers placed at 90º in two perpendicular faces of the cell. One optical fiber (model SMA905 – 400 µm in diameter, Ocean Optics, Dunedin, FL, USA) was attached to a 980nm-laser diode (model MDL-III-980-2W, Changchun New Industries Optoelectronics Technology Co., Ltd., Changchun, P.R. China) connected to a laser power supply (model PSU-III-LED). The other optical fiber (P600-025-UV-VIS - 600 µm in diameter, Ocean Optics, Dunedin, FL, USA) was attached to a modular spectrometer calibrated in the UV-VIS region (model Black-Comet, StellarNet Inc. Tampa, FL, USA). The same experimental set up was used to evaluate the nanoparticles emission at 808nm but in this case using a 808nm-laser diode (model MDL-III-808-2W, Changchun New Industries

Optoelectronics Technology Co., Ltd., Changchun, P.R. China). All samples were measured in ethanol at a concentration of 1 mg/mL and using a laser irradiance of 350 W/cm^2. The upconversion nanoparticle loading within PLGA-PEG nanoparticles was determined by thermogravimetric analysis (TGA, model Q5000IR, TA Instruments, New Castle, DE, USA) using a 10 ºC/min heating rate under a nitrogen atmosphere.

Subcytotoxic dose determination and photodynamic *in vitro* effects mediated by ROS. Human dermal fibroblasts (Lonza, Belgium), B16F1 mouse melanoma cells (kindly donated by Dr Pilar Martin-Duque), HaCaT human keratinocytes (Lonza, Belgium) and U251MG Glioblastoma (Cancer Research-UK) cell lines were grown using Dulbecco's modified Eagle's medium high glucose (DMEM w/stable Glutamine, Biowest) supplemented with fetal bovine serum (FBS, 10% (v/v); Thermo Fisher Scientific) and antibiotic-antimycotic (60 µg/mL penicillin, 100 µg/mL streptomycin and 0.25 µg/mL amphotericin B, Biowest) in a humidified atmosphere containing 5% CO_2 at 37ºC. THP-1 cell line (human acute monocytic leukemia suspension cell) was purchased from American type Culture Collection (ATCC, TIB-202™; Manassas, VA) and cultured in RPMI 1640 medium (Gibco, Thermo Fisher Scientific) supplemented with fetal bovine serum (FBS, 10% (v/v); Thermo Fisher Scientific), non-essential aminoacids (1%; Biowest), sodium piruvate (1 mM; Biowest), HEPES (10 mM; Biowest 2-mercaptoethanol (0.05 mM, Gibco, Thermo Fisher Scientific), stable glutamine (2 mM; Biowest) and antibiotic-antimycotic (60 µg/mL penicillin, 100 µg/mL streptomycin and 0.25 µg/mL amphotericin B, Biowest) at 37 °C in a 5% CO_2 humidified incubator. Monocytic cells were differentiated into the adherent macrophage-like state in supplemented RPMI 1640 medium containing 1 µM phorbol 12-myristate 13-acetate (PMA, Sigma-Aldrich) for 72 h.

Mouse mesenchymal stem cells (mMSCs) (Lonza, Belgium) were cultured in Dulbecco's modified Eagle's F-12 medium (DMEM F-12, Biowest) supplemented with fetal bovine serum (FBS, 10% (v/v); Thermo Fisher Scientific), stable glutamine (2 mM; Biowest) and antibiotic-antimycotic (60 µg/mL penicillin, 100 µg/mL streptomycin and 0.25 µg/mL amphotericin B, Biowest) and maintained at 37°C in a 5% CO_2-humidified atmosphere under hypoxic conditions (3% O_2).

In vitro cytotoxicity of oleic-acid capped and SH-PEG functionalized upconversion nanoparticles as well as unloaded PLGA-PEG nanoparticles and upconversion nanoparticles encapsulated in PLGA-PEG and PLGA-PEG nanoparticles containing upconversion nanoparticles and protoporphyrin IX were evaluated using the Alamar Blue assay (Invitrogen) according to the manufacturer's instructions. B16F1, HaCaT, THP-1 monocytic cell line, U251MG, fibroblasts, and mMSCs cells (density of 5000, 5000, 30000, 5000, 6000 and 5000 cells/well, respectively) were seeded in a 96-well plate 24 h prior to incubation with the corresponding nanoparticle doses and allowed to adhere. For differentiating THP1 monocytes into macrophages, THP-1 monocytes were seeded at a density of 70,000 cells/well in 96-well plates and differentiated with phorbol 12-myristate 13-acetate (PMA) for 3 days.

Nanoparticles were added to the cells in complete growth medium at different concentrations (0.0125-0.4 mg/mL) and, then, cells were maintained in the standard culture conditions for 24 h. After incubation, cells were washed with Dulbecco's Phosphate Buffered Saline (DPBS, Biowest) and incubated with complete growth medium containing 10% (v/v) Alamar Blue reagent for 4 h. The fluorescence intensity of the medium was measured in a multi-mode Synergy HT Microplate Reader at excitation and emission wavelengths of 530 nm and 590 nm, respectively (Biotek). The potential nanoparticle interference with the method was evaluated and discarded. Cell viability

was expressed as a relative percentage to the untreated control cells value. The percentages obtained depict the average of five values. The morphology of macrophages after internalizing upconversion nanoparticles was evaluated by SEM. Cells were cultured in gelatinized glass and fixed in paraformaldehyde 4% in PBS (Affymetrix, UK) for 30 minutes. Then, samples were washed with PBS, dried and coated with a thin Pt layer. Images were recorded in an Inspect™ F50 SEM (FEI Company) in an energy range between 10-15 keV.

In order to verify the oxidative cell damage mediated by ROS generated by NIR irradiation, B16F1, human dermal fibroblasts, mMSCs and human macrophages were seeded on 24-well plates at cell densities of 40000, 45000, 50000 and 500000 cells/well, respectively. Then, PLGA-PEG NPs containing upconversion nanoparticles and Protoporphyrin IX (0.4 mg/mL) were added to the cells. After incubation for 24h, cells were irradiated with a NIR laser (808 nm; 5, 10 and 20 min at 5.2 W/cm^2). Changes in cell well temperature were also monitored to discard any thermal mediated dead. Then, cell damage was evaluated by fluorescence microscopy just after irradiation and after 24h by using the LIVE/DEAD Viability/Cytotoxicity Kit (Thermo-Fisher Scientific, USA) following the manufacturer instructions. Briefly, a solution containing 2 μM calcein AM and 4 μM ethidium homodimer-1 was added to the cells and incubated at room temperature for 30 min. Samples were evaluated in an inverted fluorescence microscope Olympus IX81 through the composition of 20 fields on each well acquired at 4X magnification to obtain a mosaic of the central area of each well. Control samples (not treated and/or irradiated) were also assayed in order to check the basal status of cells. Furthermore, samples treated with the separated NP components (i.e., just protoporphyrin, just upconversion nanoparticles or just PLGA-PEG) and irradiated were also run to verify the restricted effect of ROS damage mediated by NIR irradiation

after treatment with the final product. These separated materials were added at the same concentration present in the final NPs.

ROS generation using a red-ox sensitive probe. ROS generation was indirectly evaluated by using Dihydrorhodamine 123 (DHR123) conversion to its oxidized and cationic form (i.e., rhodamine 123) under the presence of ROS. DHR123 is nonfluorescent but its oxidized derivative (R123) emits strong green fluorescence at 530 nm[42]. A nanoparticulated dispersion of the pegylated upconversion nanoparticles at 5 mg/mL was mixed with 50 μL of 330 μM DHR123 in 1 mL of ethanol. The final dispersion was irradiated at 11 W/cm^2 (at 980 nm) to evaluate the amount of ROS generated. The generation of R123 was monitored by using fluorescence spectroscopy using excitation and emission wavelengths of 485 nm and 530 nm, respectively. As control, the influence of the light and heating caused by the irradiation were also evaluated in order to discriminate the ROS generation attributed exclusively to the nanoparticles. Sample fluorescence was quantified before and after 2 hours of irradiation or heating.

Singlet oxygen generation detection. Singlet oxygen sensor green (SOSG, Molecular Probes, Eugene, OR, USA) (100 μg) was dissolved in 33 μL of methanol. The solution was then diluted with water by a factor of 100. The final SOSG solution was added to 9 mg/mL of nanoparticle dispersion in a 1:4 volume ratio. Irradiation was performed using a laser source at 808 nm, 15 min, 800 mW/cm^2. The fluorescence of oxidized SOSG was detected using an excitation wavelength of 504 nm and an emission wavelength of 525 nm.

Ex vivo skin permeation experiment. Human skin was collected according to the ethical guidelines of the Institutional Review Board at Boston Children's Hospital and was used to assess the *ex vivo* skin penetration depth of nanoparticles during topical drug administration. Human skin with a proper size was sandwiched between the donor and acceptor chamber of the Franz

Diffusion Cell (Inner diameter: 5 mm, area: 0.262 cm^2; volume: 5 mL). The stratum corneum side of the skin was put upward touching the donor chamber. Then, 0.2 mL of each sample (saline, free PPIX at 0.0125 mg/mL or PPIX-loaded nanoparticles) were added into the donor chamber, while 5mL of phosphate buffer (pH 7.4) was filled into the receptor chamber. The temperature of the compartments was maintained at 37 °C using a circulating water bath under gentle stirring with magnetic stirrers. After a 24 h incubation period, the skin samples were taken out from the Franz cells and were embedded in O.C.T. Compound (Tissue-Tek) and rapidly cooled with dry ice. Afterward, sections were sliced with a Cryostat Leica CM3050S (slide thickness: 10μm). The skin permeation of each of the treatment groups was then observed using Zeiss LSM 710 Multiphoton Laser Scanning Confocal Microscope. DAPI was used to stain nuclei acid of the tissues.

Statistical analysis. Results are expressed as the mean ± SD. Statistical study of data was performed by using the StataSE 12 statistical software (StataCorp LP, USA). Normal distribution of the variables was analyzed by the Shapiro-Wilk test followed by the U-Mann-Whitney or Student test. Statistically significant differences among groups were considered when $p \leq 0.05$.

ACKNOWLEDGMENTS

The authors gratefully acknowledge the financial support of the ERC Consolidator Grant program (ERC-2013-CoG-614715). CIBER-BBN is an initiative funded by the VI National R&D&i Plan 2008–2011 financed by the Instituto de Salud Carlos III with the assistance of the European Regional Development Fund. We acknowledge the LMA-INA and Microscopy and Cell Culture Core Units from IACS/IIS Aragon for their instruments and staff expertise.

REFERENCES

(1) Mengjun, C.; Meizhen, Y. Design and Development of Fluorescent Nanostructures for Bioimaging. *Prog. Polym. Sci.* **2014**, *39* (2), 365–395.

(2) Wang, C.; Cheng, L.; Liu, Z. Upconversion Nanoparticles for Photodynamic Therapy and Other Cancer Therapeutics. *Theranostics* **2013**, *3* (5), 317–330.

(3) Yan, B.; Boyer, J.-C.; Branda, N. R.; Zhao, Y. Near-Infrared Light-Triggered Dissociation of Block Copolymer Micelles Using Upconverting Nanoparticles. *J. Am. Chem. Soc.* **2011**, *133* (49), 19714–19717.

(4) Jayakumar, M. K. G.; Idris, N. M.; Zhang, Y. Remote Activation of Biomolecules in Deep Tissues Using near-Infrared-to-UV Upconversion Nanotransducers. *Proc. Natl. Acad. Sci.* **2012**, *109* (22), 8483–8488.

(5) Guo, H.; Yan, D.; Wei, Y.; Han, S.; Qian, H.; Yang, Y.; Zhang, Y.; Liu, X.; Sun, S. Inhibition of Murine Bladder Cancer Cell Growth in Vitro by Photocontrollable siRNA Based on Upconversion Fluorescent Nanoparticles. *PLoS One* **2014**, *9* (11), 112713–112725.

(6) Liu, J.; Bu, W.; Pan, L.; Shi, J. NIR-Triggered Anticancer Drug Delivery by Upconverting Nanoparticles with Integrated Azobenzene-Modified Mesoporous Silica. *Angew. Chemie - Int. Ed.* **2013**, *52* (16), 4375–4379.

(7) Jalani, G.; Naccache, R.; Rosenzweig, D. H.; Haglund, L.; Vetrone, F.; Cerruti, M. Photocleavable Hydrogel-Coated Upconverting Nanoparticles: A Multifunctional Theranostic Platform for NIR Imaging and On-Demand Macromolecular Delivery. *J. Am. Chem. Soc.* **2016**, *138* (3), 1078–1083.

(8) Zhang, L.; Zeng, L.; Pan, Y.; Luo, S.; Ren, W.; Gong, A.; Ma, X.; Liang, H.; Lu, G.; Wu, A. Inorganic Photosensitizer Coupled Gd-Based Upconversion Luminescent

Nanocomposites for Invivo Magnetic Resonance Imaging and near-Infrared-Responsive Photodynamic Therapy in Cancers. *Biomaterials* **2015**, *44*, 82–90.

(9) Xu, J.; Yang, P.; Sun, M.; Bi, H.; Liu, B.; Yang, D.; Gai, S.; He, F.; Lin, J. Highly Emissive Dye-Sensitized Upconversion Nanostructure for Dual-Photosensitizer Photodynamic Therapy and Bioimaging. *ACS Nano* **2017**, *11* (4), 4133–4144.

(10) Juzenas, P.; Juzeniene, A.; Kaalhus, O.; Iani, V.; Moan, J. Noninvasive Fluorescence Excitation Spectroscopy during Application of 5-Aminolevulinic Acid in Vivo. *Photochem. Photobiol. Sci.* **2002**, *1* (10), 745–748.

(11) Weissleder, R. A Clearer Vision for in Vivo Imaging. *Nat. Biotechnol.* **2001**, *19* (4), 316–317.

(12) Ding, M.; Lu, C.; Cao, L.; Ni, Y.; Xu, Z.; Li, C.; Lin, J.; Wang, W.; Li, C.; Cheng, Z.; Lin, J.; Ni, D.; He, Q.; Shi, J. Controllable Synthesis, Formation Mechanism and Upconversion Luminescence of ?-NaYF4?:?Yb3+/Er3+ Microcrystals by Hydrothermal Process. *CrystEngComm* **2013**, *15* (41), 8366–8373.

(13) Wang, F.; Deng, R.; Wang, J.; Wang, Q.; Han, Y.; Zhu, H.; Chen, X.; Liu, X. Tuning Upconversion through Energy Migration in Core–shell Nanoparticles. *Nat. Mater.* **2011**, *10* (12), 968–973.

(14) Zhang, L.; He, R.; Gu, H. C. Oleic Acid Coating on the Monodisperse Magnetite Nanoparticles. *Appl. Surf. Sci.* **2006**, *253* (5), 2611–2617.

(15) Cao, C.; Qin, W.; Zhang, J.; Wang, Y.; Zhu, P.; Wei, G.; Wang, G.; Kim, R.; Wang, L. Ultraviolet Upconversion Emissions of Gd3+. *Opt. Lett.* **2008**, *33* (8), 857–859.

(16) Pollnau, M.; Gamelin, D. R.; Lüthi, S. R.; Güdel, H. U.; Hehlen, M. P. Power Dependence of Upconversion Luminescence in Lanthanide and Transition-Metal-Ion Systems. *Phys.*

Rev. B **2000**, *61* (5), 3337–3346.

(17) Boyer, J.-C.; Carling, C.-J.; Gates, B. D.; Branda, N. R. Two-Way Photoswitching Using One Type of Near-Infrared Light, Upconverting Nanoparticles, and Changing Only the Light Intensity. *J. Am. Chem. Soc.* **2010**, *132* (44), 15766–15772.

(18) Liu, L.; Jiang, H.; Chen, Y.; Zhang, X.; Zhang, Z.; Wang, Y. Power Dependence of Upconversion Luminescence of Er3+ Doped Yttria Nanocrystals and Their Bulk Counterpart. *J. Lumin.* **2013**, *143*, 423–431.

(19) Li, X.; Zhang, F.; Zhao, D. Lab on Upconversion Nanoparticles: Optical Properties and Applications Engineering via Designed Nanostructure. *Chem. Soc. Rev.* **2015**, *44* (6), 1346–1378.

(20) Wang, Y.-F.; Liu, G.-Y.; Sun, L.-D.; Xiao, J.-W.; Zhou, J.-C.; Yan, C.-H. Nd^{3+} -Sensitized Upconversion Nanophosphors: Efficient *In Vivo* Bioimaging Probes with Minimized Heating Effect. *ACS Nano* **2013**, *7* (8), 7200–7206.

(21) Guo, S.; Xie, X.; Huang, L.; Huang, W. Sensitive Water Probing through Nonlinear Photon Upconversion of Lanthanide-Doped Nanoparticles. *ACS Appl. Mater. Interfaces* **2016**, *8* (1), 847–853.

(22) Hatakeyama, T.; Murayama, Y.; Komatsu, S.; Shiozaki, A.; Kuriu, Y.; Ikoma, H.; Nakanishi, M.; Ichikawa, D.; Fujiwara, H.; Okamoto, K.; Ochiai, T.; Kokuba, Y.; Inoue, K.; Nakajima, M.; Otsuji, E. Efficacy of 5-Aminolevulinic Acid-Mediated Photodynamic Therapy Using Light-Emitting Diodes in Human Colon Cancer Cells. *Oncol. Rep.* **2013**, *29* (3), 911–916.

(23) da Silva, C. L.; Del Ciampo, J. O.; Rossetti, F. C.; Bentley, M. V. L. B.; Pierre, M. B. R. PLGA Nanoparticles as Delivery Systems for Protoporphyrin IX in Topical PDT:

Cutaneous Penetration of Photosensitizer Observed by Fluorescence Microscopy. *J. Nanosci. Nanotechnol.* **2013**, *13* (10), 6533–6540.

(24) Ortiz de Solorzano, I.; Prieto, M.; Mendoza, G.; Alejo, T.; Irusta, S.; Sebastian, V.; Arruebo, M. Microfluidic Synthesis and Biological Evaluation of Photothermal Biodegradable Copper Sulfide Nanoparticles. *ACS Appl. Mater. Interfaces* **2016**, *8* (33), 21545–21554.

(25) Chernikov, A. V.; Bruskov, V. I.; Gudkov, S. V. Heat-Induced Formation of Nitrogen Oxides in Water. *J. Biol. Phys.* **2013**, *39* (4), 687–699.

(26) Gnach, A.; Lipinski, T.; Bednarkiewicz, A.; Rybka, J.; Capobianco, J. A.; Wang, L.; Ewing, R. C.; Wang, J.; Bai, D.; Zeng, Z.; Magdeleine, E.; Gros-Dagnac, H.; Celsis, P.; Mauricot, R.; Shi, J.; Cuschieri, J.; Bankey, P. E.; Johnson, J. L.; Sperry, J.; Nathens, A. B.; Billiar, T. R.; West, M. A.; Jeschke, M. G.; Klein, M. B.; Gamelli, R. L.; Gibran, N. S.; Brownstein, B. H.; Miller-Graziano, C.; Calvano, S. E.; Mason, P. H.; Cobb, J. P.; Rahme, L. G.; Lowry, S. F.; Maier, R. V.; Moldawer, L. L.; Herndon, D. N.; Davis, R. W.; Xiao, W.; Tompkins, R. G.; Injury, T. I. L. S. C. R. P. H. R. to. Upconverting Nanoparticles: Assessing the Toxicity. *Chem. Soc. Rev.* **2015**, *44* (6), 1561–1584.

(27) ISO/TC 194. ISO 10993-5:2009, Biological Evaluation of Medical Devices Part 5: Tests for in Vitro Cytotoxicity. International Organization for Standardization 2009.

(28) Aderem, A.; Underhill, D. M. MECHANISMS OF PHAGOCYTOSIS IN MACROPHAGES. *Annu. Rev. Immunol.* **1999**, *17* (1), 593–623.

(29) Shimoyama, A.; Watase, H.; Liu, Y.; Ogura, S.-I.; Hagiya, Y.; Takahashi, K.; Inoue, K.; Tanaka, T.; Murayama, Y.; Otsuji, E.; Ohkubo, A.; Yuasa, H. Access to a Novel near-Infrared Photodynamic Therapy through the Combined Use of 5-Aminolevulinic Acid and

Lanthanide Nanoparticles. *Photodiagnosis Photodyn. Ther*. **2013**, *10* (4), 607–614.

(30) Tian, G.; Ren, W.; Yan, L.; Jian, S.; Gu, Z.; Zhou, L.; Jin, S.; Yin, W.; Li, S.; Zhao, Y. Upconversion: Red-Emitting Upconverting Nanoparticles for Photodynamic Therapy in Cancer Cells Under Near-Infrared Excitation (Small 11/2013). *Small* **2013**, *9* (11), 1928–1928.

(31) Xing, H.; Bu, W.; Ren, Q.; Zheng, X.; Li, M.; Zhang, S.; Qu, H.; Wang, Z.; Hua, Y.; Zhao, K.; Zhou, L.; Peng, W.; Shi, J. A NaYbF4: Tm3+ Nanoprobe for CT and NIR-to-NIR Fluorescent Bimodal Imaging. *Biomaterials* **2012**, *33* (21), 5384–5393.

(32) Bacellar, I.; Tsubone, T.; Pavani, C.; Baptista, M. Photodynamic Efficiency: From Molecular Photochemistry to Cell Death. *Int. J. Mol. Sci.* **2015**, *16* (9), 20523–20559.

(33) Kankala, R. K.; Liu, C.-G.; Chen, A.-Z.; Wang, S.-B.; Xu, P.-Y.; Mende, L. K.; Liu, C.-L.; Lee, C.-H.; Hu, Y.-F. Overcoming Multidrug Resistance through the Synergistic Effects of Hierarchical pH-Sensitive, ROS-Generating Nanoreactors. *ACS Biomater. Sci. Eng.* **2017**, *3* (10), 2431–2442.

(34) Kankala, R. K.; Kuthati, Y.; Liu, C.-L.; Lee, C.-H. Hierarchical Coated Metal Hydroxide Nanoconstructs as Potential Controlled Release Carriers of Photosensitizer for Skin Melanoma. *RSC Adv.* **2015**, *5* (53), 42666–42680.

(35) Hempstead, J.; Jones, D. P.; Ziouche, A.; Cramer, G. M.; Rizvi, I.; Arnason, S.; Hasan, T.; Celli, J. P. Low-Cost Photodynamic Therapy Devices for Global Health Settings: Characterization of Battery-Powered LED Performance and Smartphone Imaging in 3D Tumor Models. *Sci. Rep.* **2015**, *5*, 10093–10105.

(36) Nemes, A.; Fortmann, T.; Poeschke, S.; Greve, B.; Prevedello, D.; Santacroce, A.; Stummer, W.; Senner, V.; Ewelt, C. 5-ALA Fluorescence in Native Pituitary Adenoma Cell

Lines: Resection Control and Basis for Photodynamic Therapy (PDT)? *PLoS One* **2016**, *11* (9), 161364–161375.

(37) Nakayama, T.; Otsuka, S.; Kobayashi, T.; Okajima, H.; Matsumoto, K.; Hagiya, Y.; Inoue, K.; Shuin, T.; Nakajima, M.; Tanaka, T.; Ogura, S.-I. Dormant Cancer Cells Accumulate High Protoporphyrin IX Levels and Are Sensitive to 5-Aminolevulinic Acid-Based Photodynamic Therapy. *Sci. Rep.* **2016**, *6*, 36478–36489.

(38) Moan, J.; Berg, K. The Photodegradation of Porphyrins in Cells Can Be Used to Estimate the Lifetime of Singlet Oxygen. *Photochem. Photobiol.* **1991**, *53* (4), 549–553.

(39) Rossetti, F. C.; Depieri, L. V.; Tedesco, A. C.; Bentley, M. V. L. B. Fluorometric Quantification of Protoporphyrin IX in Biological Skin Samples from in Vitro Penetration/permeation Studies. *Brazilian J. Pharm. Sci.* **2010**, *46* (4), 753–760.

(40) Liu, B.; Deng, X.; Xie, Z.; Cheng, Z.; Yang, P.; Lin, J. Thiol-Ene Click Reaction as a Facile and General Approach for Surface Functionalization of Colloidal Nanocrystals. *Adv. Mater.* **2017**, *29* (36), 1604878–1604887.

(41) Jokerst, J. V; Lobovkina, T.; Zare, R. N.; Gambhir, S. S. Nanoparticle PEGylation for Imaging and Therapy. *Nanomedicine* **2011**, *6* (4), 715–728.

(42) Crow, J. P. Dichlorodihydrofluorescein and Dihydrorhodamine 123 Are Sensitive Indicators of Peroxynitrite in Vitro: Implications for Intracellular Measurement of Reactive Nitrogen and Oxygen Species. *Nitric Oxide* **1997**, *1* (2), 145–157.